α_1-Antitrypsin Polymerization: A Fluorescence Correlation Spectroscopic Study†

Pradipta Purkayastha, Jason W. Klemke, Stacey Lavender, Rolando Oyola, Barry S. Cooperman, and Feng Gai*

Department of Chemistry, University of Pennsylvania, Philadelphia, Pennsylvania 19104

Received June 26, 2004; Revised Manuscript Received October 8, 2004

ABSTRACT: α_1-Antitrypsin (AT) is the most abundantly circulating human proteinase inhibitor in the serpin family. The polymerization of AT, leading to α_1-antitrypsin deficiency, has been studied extensively in vitro by a variety of ensemble methods. Here we report the use of fluorescence correlation spectroscopy to gain further insight into this process. Measurements of the distributions of diffusion times of polymerizing AT, carried out at 45, 50, and 55 °C, clearly show the existence of a kinetic lag phase, during which short oligomers are formed, prior to the formation of heterogeneous mixtures of longer polymers, and suggest that long polymers, which appear to be metastable, are produced through the condensation of shorter oligomers.

The serine proteinase inhibitors (serpins) are a superfamily of proteins that control a wide variety of biological events, such as inflammation, coagulation, and fibrinolysis (*1*−*3*). This superfamily contains a diverse set of proteins, including α_1-antitrypsin (AT),[1] α_1-antichymotrypsin, C1 inhibitor, antithrombin, and plasminogen activator inhibitor-1 (*4*, *5*). Crystal structures of serpins have shown that they are comprised of a highly conserved tertiary fold consisting of three large β-sheets surrounded by nine α-helices, and a reactive center loop containing the scissile bond denoted as P_1-P_1' (residues 358−359) (*6*−*9*) (Figure 1). Within this fold, the reactive center loop is the most flexible element and can remain either totally exposed or become partly or fully inserted into the center of the A β-sheet (*9*−*12*). This flexibility, while apparently critical for serpin inhibitory function (*2*), can also lead to serpin polymerization, the underlying cause of several diseases (*13*, *14*). While mutations in serpins can induce polymerization even under physiological conditions, polymerization of native serpins typically requires incubation either at temperatures higher than 40 °C or in the presence of relatively low concentrations of denaturants, such as guanidine hydrochloride (*15*−*17*).

AT is the most abundantly circulating proteinase inhibitor (*18*−*20*) among human serpins. Polymerization of AT leads to α_1-antitrypsin deficiency, which may further result in juvenile cirrhosis, hepatocellular carcinoma (*21*, *22*), or early-onset panlobular emphysema (*23*, *24*). AT polymerization has been studied extensively in vitro. The overall process is temperature and concentration dependent (*18*, *25*, *26*), and gives rise to polymers resembling "beads on a string", as determined by electron microscopy (*27*). Studies employing fluorescence and circular dichroism (CD) spectroscopy have led to the suggestion that AT polymerization follows a bi-

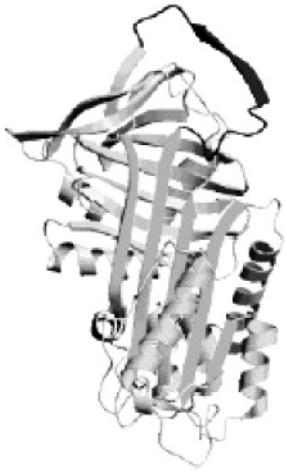

FIGURE 1: Crystal structure of α_1-antitrypsin showing the reactive center loop (top) and the A β-sheet (front) (*9*).

phasic mechanism, in which a rapid unimolecular step involving a conformational change is followed by a bimolecular interaction involving insertion of the reactive center loop of one molecule into the A β-sheet of a second molecule (*25*, *26*). A recent study, conducted at pH 4, and employing turbidity measurements in addition to florescence and CD, provides evidence for a more complex mechanism, in which the first-order step is followed by two bimolecular reactions, with the formation of a protodimer corresponding to loop insertion into the C β-sheet rather than the A β-sheet (*28*−*30*).

Although these latter studies, employing ensemble-averaged approaches, provide significant insight into AT polymerization, they are incapable of elucidating many aspects of the mechanism, in particular the distributions of stable products and transient intermediates during polymerization. By contrast, fluorescence correlation spectroscopy (FCS), which allows the detection of single molecules, can be used to determine these distributions. FCS (*31*−*37*) is based on the measurement of temporal intensity fluctuations caused by one or several fluorescent molecules diffusing in and out

† Supported by the NIH (GM-065978 and AG-10599).

* To whom correspondence should be addressed. E-mail: gai@sas.upenn.edu.

[1] AT, α_1-antitrypsin; TMR, tetramethylrhodamine; EDTA, ethylenediaminetetraacetic acid; PMSF, phenylmethylsulfonylfluoride; PAGE, polyacrylamide gel electrophoresis; FCS, fluorescence correlation spectroscopy.

10.1021/bi048662e CCC: $30.25
Published on Web 01/28/2005

of a well-defined excitation volume element. The autocorrelation function obtained from the intensity fluctuations provides information about the residence time of a fluorescent molecule in the excitation volume element, allowing calculation of the molecule's diffusion constant and hydrodynamic radius, based on the Stokes−Einstein relationship (*38*, *39*). From the amplitude of the autocorrelation function one can also obtain the number of molecules within the volume element, and thus the sample concentration (*40*−*42*).

FCS has previously been used to study reactions such as DNA-induced polymerization of HIV-1 integrase (*35*), the elongation and branching of fibrinogen polymers induced by thrombin (*36*) and the aggregation properties of amyloid β-protein (*31*, *32*). Here we employ FCS to elucidate the mechanism of AT polymerization. Our results demonstrate that polymerization proceeds via a lag phase, corresponding to the accumulation of small oligomers, which is followed by a rather abrupt formation of considerably larger aggregates.

MATERIALS AND METHODS

Preparation of the C232S/S359C α1-Antitrypsin Variant. Site directed mutagenesis was accomplished using the Quickchange method (Stratagene, La Jolla, CA). The template was a double-stranded pET11a vector (New England Biolabs, Beverly, MA) containing T7 promoter, terminator and the entire antitrypsin cDNA. Primers were annealed to the template using *Pfu* DNA polymerase and thermal cycling. The PCR product was transformed into XL-1 supercompetent cells. Plasmid DNA was isolated using either the Wizard Plus SV DNA purification system (Promega, Madison, WI) or the Qiagen Plasmid mini kit. Mismatched codons were confirmed by DNA sequencing.

Expression. E. coli strain BL21 containing pET-pro-AT was grown at 37 °C in 15 L of LB medium containing 0.1 mg/mL ampicillin. When A_{600} reached 0.4−1.0, isopropyl-β-D-thiogalactose was added at 1 mM final concentration to induce pro-rAT expression, and growth was continued for another 3−4 h, bacterial cells were harvested, quickly frozen, and stored at −70 °C.

Purification. Approximately 20 g of cell paste was dispersed in 200 mL of buffer A (50 mM Tris, pH 7.8, 50 mM NaCl, 1 mM EDTA, 10 mM β-mercaptoethanol). Phenylmethylsulfonylfluoride (PMSF) was added to a final concentration of 150 mM. Cells were lysed by passage through a French press at 10,000 psi at 4 °C. Supernatant was collected and centrifuged at 10,000 rpm for 35 min. The pellet, containing recombinant α1-antitrypsin within inclusion bodies, was washed 2x with buffer A containing 0.5% Triton X-100, and then dissolved in buffer A containing 8 M urea. Solubilized protein was diluted to 2 L of refolding buffer, buffer B (10 mM sodium phosphate, pH 6.5, 50 mM NaCl, 1 mM EDTA and 1 mM β-mercaptoethanol). The protein concentration was ∼ 0.4 mg/mL. After incubating overnight at 4 °C, the solution was dialyzed against 30 L of buffer B with three changes. The dialyzed sample was applied to a DEAE-Sepharose column (2.5 × 50 cm) (BioRad, Hercules, CA) and eluted with 0−0.3 M NaCl linear gradient. Fractions containing α1-antitrypsin were pooled, concentrated and buffer-exchanged using an Amicon concentrator. The purified sample contains only a small amount (<20%) of dimers and/or trimers, as shown by PAGE analysis. The activity of the refolded protein was confirmed by its ability to inhibit chymotrypsin enzymatic activity.

Preparation of P1′-TMR-AT. C232S/S359C-α1-antitrypsin (1.3 mg) was reacted with a 20-fold excess of tetramethylrhodamine (TMR) dye and a 10-fold excess of buffer C (tris-(2-carboxyethyl)phosphine hydrochloride (Molecular Probes) in 5 mL of 50 mM Tris/50 mM KCl buffer, pH 8.3). The reaction proceeded overnight at 4 °C in the dark, and was quenched by addition of excess β-mercaptoethanol. Excess dye was removed by applying the reaction mixture to a column (5.0 cm) consisting of 8.3 mL of PD-10 (Amersham Biosciences, Piscataway, NJ) topped by 1.0 mL of Toyopearl HW-40C (Tosoh Bioscience, Inc., South San Francisco, CA). AT-containing fractions were pooled, concentrated, and reapplied to the column for further removal of excess dye. The extent of labeling of AT at the P1′ position is 1.04 TMR/protein, as determined using a TMR extinction coefficient of 52,000 M^{-1} cm^{-1} at its isosbestic point (528 nm) (*43*). Protein was measured by bicinchoninic acid (BCA, Pierce, Rockford, IL) assay.

PAGE Analysis of α1-Antitrypsin Polymerization. α1-Antitrypsin (18.0 μM) of sample was heated to the desired temperature in buffer C, aliquots were removed at various time points, and brought to room temperature by dilution with 5 volumes of buffer C. Samples were analyzed by nondenaturing polyacrylamide gradient gels (4−15%, Bio-Rad, Hercules, CA). Protein was visualized by silver staining. Densiometric analysis was performed using NIH Image software, version 1.61.

Fluorescence Correlation Spectroscopy. The confocal fluorescence microscope used is similar to those described in other studies (*35*−*37*, *44*). Briefly, the excitation source (∼270 μW) at 514.5 nm was derived from the laser lines of an Ar^+ laser (Spectra-Physics, Mt. View, CA), which was brought to a focus in the sample solution by a microscope objective (Nikon 100×, NA 1.3, oil-immersion). The emission was collected by the same objective and was separated from the excitation by a dichroic mirror. The confocal volume was defined by a 50 μm pinhole. A single interference filter was used to allow only the fluorescence to pass through and reach the detector. Photon counting in real time was done by an avalanche photodiode detector (SPCM-AQR-16, Perkin-Elmer, Vaudreuil, Canada) and a data acquisition card (PCI-6602, National Instruments, Austin, TX). A computer program written in LABVIEW (National Instruments, Austin, TX) was used to control the data collection as well as the subsequent autocorrelation analysis.

For a prolate ellipsoidal Gaussian observation volume the autocorrelation function $G(\tau)$ is given by eq 1 (*45*, *46*):

$$G(\tau) = \frac{1}{N}\sum_{i=1}^{n}\left(\frac{f_i}{1+\frac{\tau}{\tau_D{}^i}}\right)\left(\frac{1}{1+\frac{\tau}{\omega^2\tau_D{}^i}}\right)^{1/2} \quad (1)$$

where n represents the number of fluorescent species in solution, τ is the lag time, $\tau_D{}^i$ is the characteristic diffusion time of species i during which it resides in the observation volume, ω signifies the axial (z_0) to lateral (r_0) dimension ratio of the volume element, N denotes the mean number of

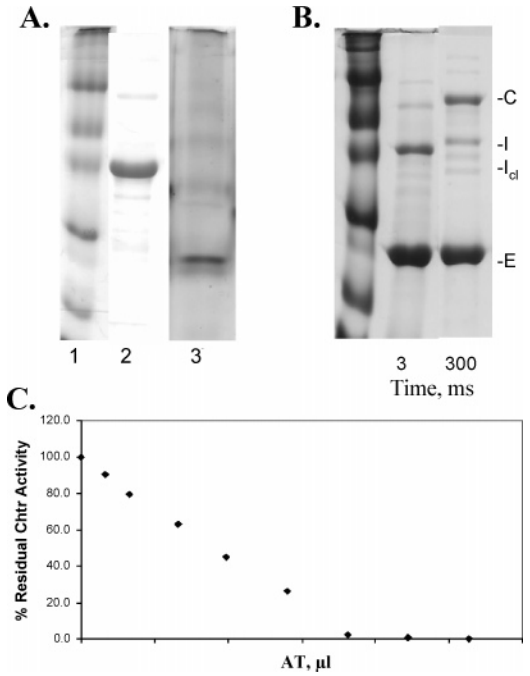

FIGURE 2: Characterization of P1′-AT. (A) Gel electrophoretic analysis of purified protein. Lanes 1 and 2, SDS−PAGE, standards and purified protein, respectively, Coomassie blue staining. Lane 3, nondenaturing PAGE, purified protein, silver staining. (B) SDS−PAGE analysis of complex formation between P1′-AT (10.0 μM) and chymotrypsin (30.0 μM). Samples were mixed in a quenched flow apparatus. E, chymotrypsin; I, P1′-AT; I_{cl}, cleaved P1′-AT; C, chymotrypsin−P1′-AT complex. (C) Inhibition of chymotrypsin activity by P1′-ACT.

fluorescent molecules in the time limit $\tau \rightarrow 0$, i.e., $G(\tau \rightarrow 0) = 1/N$, and f_i signifies the fraction of species i in the solution. Since τ_D for a given molecule correlates with its hydrodynamic radius, it can be used to monitor the kinetics of a polymerization process during which slower diffusing species are generated.

Samples for FCS analysis were prepared by quickly heating 5 μM P1′-TMR-AT in buffer D (50 mM Tris-KCl buffer, pH 8.3) to the desired temperature (e.g., 45, 50, or 55 °C), which was maintained over the course of the experiment. At predetermined time intervals aliquots were removed, quickly diluted with buffer solution at room temperature (23 °C) to give a final concentration of 1 nM. This procedure halts further polymerization or depolymerization (*30*). Diluted samples were used immediately for FCS measurements. The total observation time for each FCS measurement is 100 s with an integration time of 100 μs for each point. Either 10 (for data presented in Figure 7) or 100 (for data presented in Figure 8) measurements were taken for each diluted sample.

RESULTS

Characterization of C232S/S359C-α_1-antitrypsin (P1′-AT). P1′-AT was purified to apparent near homogeneity when analyzed by SDS−PAGE, but showed the clear presence of small amounts of aggregates, presumably mostly dimer and trimer, when analyzed in a nondenaturing gradient gel (Figure 2A). The large majority of the protein is active in formation of an SDS-stable complex with chymotrypsin, with only minor concomitant formation of cleaved P1′-AT (Figure 2B). The apparent stoichiometry of inhibition (SI) value for

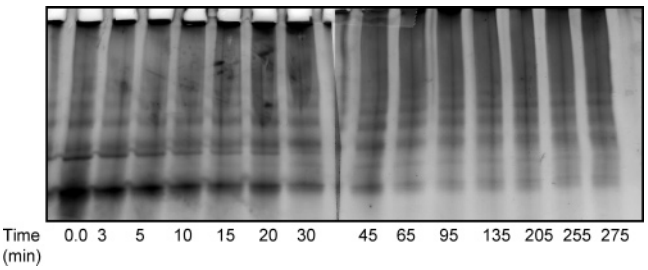

FIGURE 3: Nondenaturing gel analysis of TMR−P1′-AT polymerization at 55 °C. TMR−P1′-AT (0.8 mg/mL) was incubated in buffer C. At the times indicated, aliquots were removed, diluted 5-fold in 50 mM Tris, 50 mM KCl buffer, pH 8.3, and flash frozen in liquid nitrogen. A 4−15% gradient gel was employed.

P1′-AT vs chymotrypsin is 1.3, as determined by densitometric scanning of gels such as those shown in Figure 2B (*47*) and by titration (Figure 2C).

Nondenaturing PAGE Analysis of Ensemble P1′-AT Polymerization. Nondenaturing PAGE analysis provides an ensemble approach for following heat-induced P1′-AT polymerization (*18*, *25*). As seen in Figure 3 for TMR−P1′-AT, as time increases, there is a clear and easily quantifiable disappearance of the dominant monomer band, as well as a darkening of the upper portion of the gel, consistent with the formation of a heterodisperse mixture of protein aggregates. Similar results were obtained for P1′-AT. Comparison of the rates of disappearance of P1′-AT monomer and TMR−P1′-AT monomer at 55 °C, and of the rates of disappearance of P1′-AT monomer at 45 °C and 65 °C as well (Figure 4), make it clear that the apparent rate constant (a) is insensitive to TMR substitution at P1′ [$0.61 \pm 0.05 \times 10^{-3}$ s^{-1} (P1′-AT) vs $0.68 \pm 0.07 \times 10^{-3}$ s^{-1} (TMR−P1′-AT)] and (b) is very temperature sensitive, rising 50-fold with a 20 °C rise in temperature (45 °C to 65 °C), and giving an activation energy of 175 kJ/mol (Figure 4, inset).

It is worth noting that the apparent rate constant for P1′-AT monomer disappearance at 45 °C, 0.05×10^{-3} s^{-1}, is similar in magnitude to the narrow range of values ($0.03-0.04 \times 10^{-3}$ s^{-1}) previously determined at the same temperature for a slow phase of polymerization of human plasma AT, using three different ensemble fluorescence measurements (*29*). It would thus appear that the minor contamination of P1′-AT monomer with dimer and trimer, noted above, has no major accelerating effect on P1′-AT polymerization. This is consistent with recent results showing that the rate of AT aggregation, unlike that of ACT aggregation, is not nucleated by α-Crystallin (*48*).

FCS Measurements. Sample FCS measurements (photon bursts) for an unheated sample of P1′-TMR-AT are shown in Figure 5. The autocorrelation of these signals can be modeled by eq 1 with two components (Figure 6). The fast component has a diffusion time of ~200 μs, which is quite likely due to a small amount of residual free dye molecules, whereas the major slow component has a diffusion time of ~2 ms and can be assigned to the diffusion of the monomer. This assignment is consistent with the theoretically estimated diffusion time of the AT monomer, which has a hydrodynamic radius of about 35 Å (*49*), based on the Stokes−Einstein relationship (*42*). The diffusion coefficient of Rhodamine 6G has been determined to be 2.8×10^{-6} cm^2 s^{-1} (*42*). Using this value as a standard, the diffusion

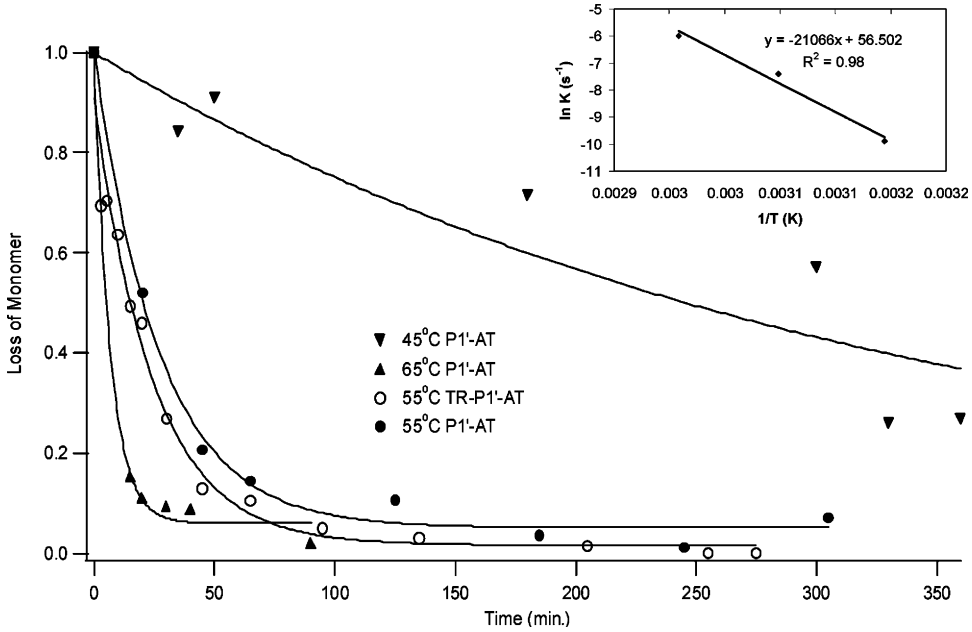

FIGURE 4: Rate of monomer disappearance. Gels were scanned and densiometric analysis of monomer intensity was performed using NIH Image 1.61. Lines are drawn to calculate first-order rate constants. Inset shows an Arrhenius plot for P1′-AT rate constants.

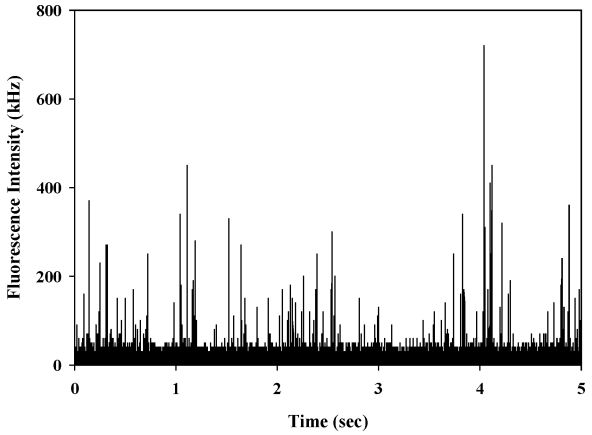

FIGURE 5: Fluorescence signal from TMR labeled AT monomer as a function of time. $\lambda_{ex} = 514.5$ nm.

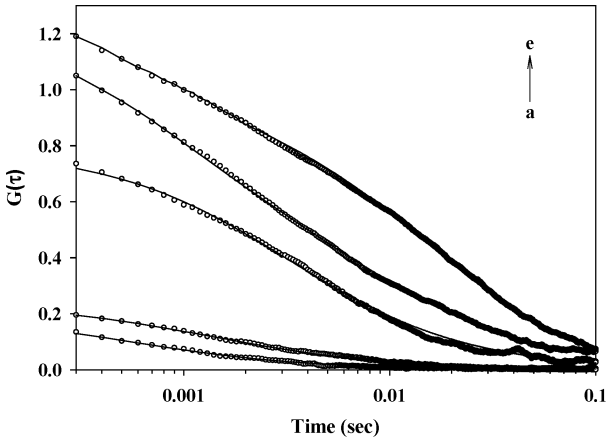

FIGURE 6: Representative autocorrelation decay profiles (○) corresponding to different reaction times of the polymerization reaction of AT at 45 °C: (a) 0 min; (b) 200 min; (c) 465 min; (d) 675 min; (e) 49 h. Solid lines are fits to eq 1.

coefficient of the AT monomer was determined to be 3.2×10^{-8} cm^2 s^{-1} according to the following relationship:

$$\frac{D_{\text{rhodamine}}}{D_{\text{monomer}}} = \frac{\tau_{\text{rhodamine}}}{\tau_{\text{monomer}}} \qquad (2)$$

where D is the diffusion coefficient and τ is the respective diffusion time. As a control, we have also measured the diffusion time of TMR (data not shown). The recovered τ_D (~200 μs) was similar to that measured by others using comparable equipments (*35*−*37*, *44*).

Autocorrelation Decay. The autocorrelation data in Figure 6 present two indications that P1′-TMR-AT polymerizes on prolonged incubation at 45 °C. First, the rate constant for decay of the slow component decreases, indicating formation of slower diffusing species due to polymerization. Second, $G(0)$, the amplitude of the autocorrelation function, which is inversely proportional to the average number of species in the confocal volume at zero time, increases, consistent with monomer disappearance. Moreover, this increase occurs with a rate constant of $0.05 \pm 0.01 \times 10^{-3}$ s^{-1}, which agrees precisely with the ensemble rate constant for monomer disappearance mentioned above (Figure 4).

Diffusion Time Distribution. The distributions of diffusion times as a function of reaction time, temperature, and initial AT concentration are shown in Figure 7. At 45 °C, species with diffusion times of 4 to 6 ms are quickly formed (<30 min). This initial distribution remains essentially unchanged for about 200 min, after which there is a clear increase in the population of species whose diffusion times are between 8 and 16 ms. Most interesting, however, is the sudden jump in the diffusion time at about 400 min, indicating the formation of longer polymers. After this point, the population of these long polymers continues to increase. These results are consistent with the widely held notion (*26*) that serpin polymerization proceeds via a lag phase, during which shorter oligomers are formed. A more detailed examination of the transition from shorter to longer polymers is displayed in Figure 7b, in which FCS measurements were carried out on aliquots removed at 15 min intervals on either side of the 400 min incubation time. The results indicate that the marked

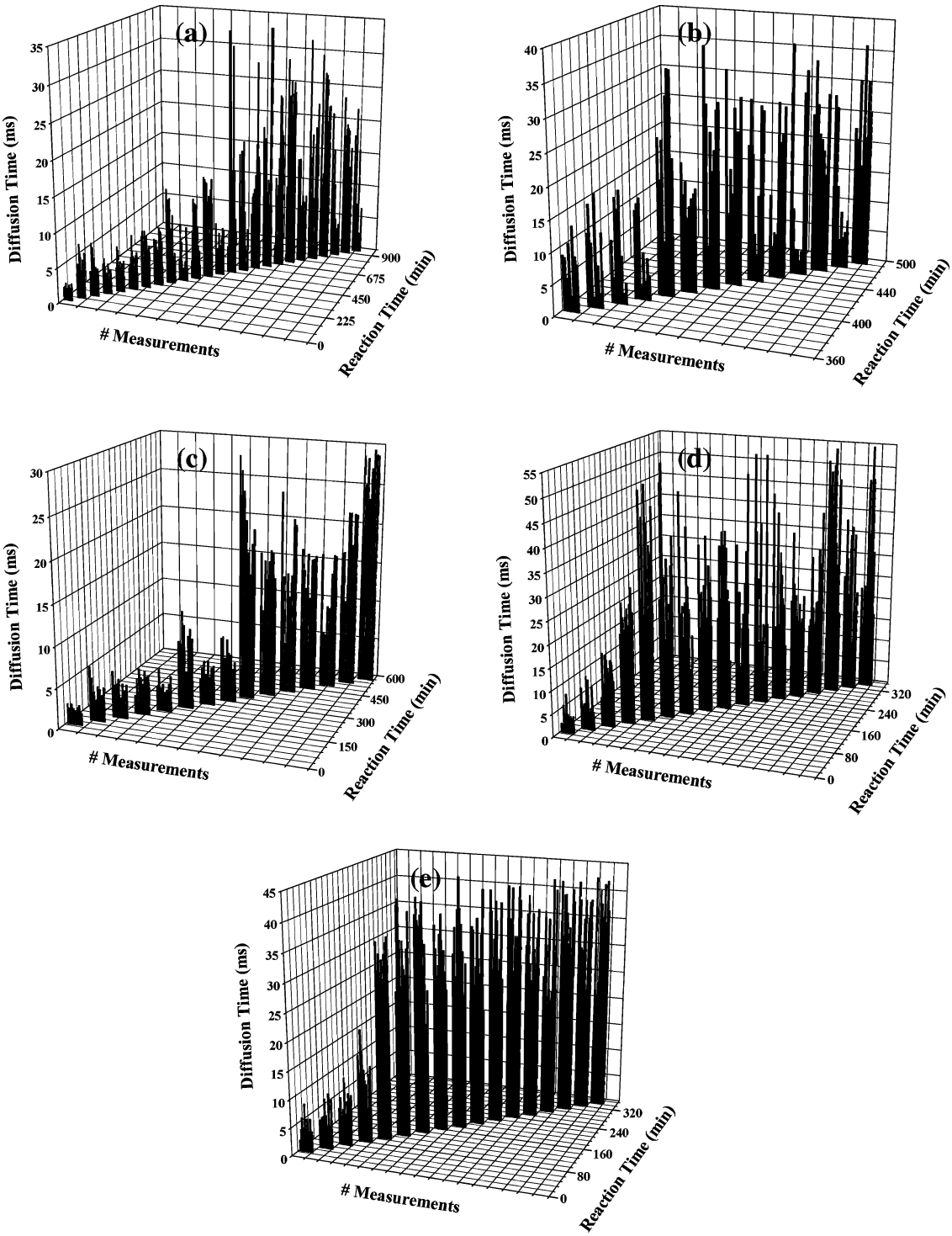

FIGURE 7: Distribution of diffusion times of polymerization of AT with the progress of the reaction at different temperatures and initial AT concentrations. Temperature: (a and e) 45 °C; (c) 50 °C; (d) 55 °C. Concentration: (a, c, and d) 5 μM; (e) 22 μM. The distribution of diffusion times at the point of long chain formation at 45 °C and 5 μM AT is displayed in part b.

rise in diffusion time takes less than 15 min, strongly suggesting that longer AT polymers are generated by the fusions of two shorter polymers. This suggestion is consistent with models used by Bark et al. (*36*).

AT polymerization at 50 and 55 °C, (Figure 7c and d), proceeds similarly to the process at 45 °C except the length of the lag phase preceding formation of long polymers decreases. In addition, polymers formed at 55 °C have considerably longer diffusion times on average, as compared with those formed at 45 and 50 °C. Raising the initial concentration of AT from 5 to 22 μM at 45 °C (Figure 7e) also decreases the length of the initial lag phase, by about 4-fold. However, the resulting polymers display a narrower chain length distribution, with a markedly higher percentage of the longer polymeric strands and an increased average chain length as compared with what is seen at lower concentration (Figure 7a). These changes most likely reflect a change in the position of equilibrium between longer and shorter polymers as a function of concentration. While the effects of increasing temperature and AT concentration on

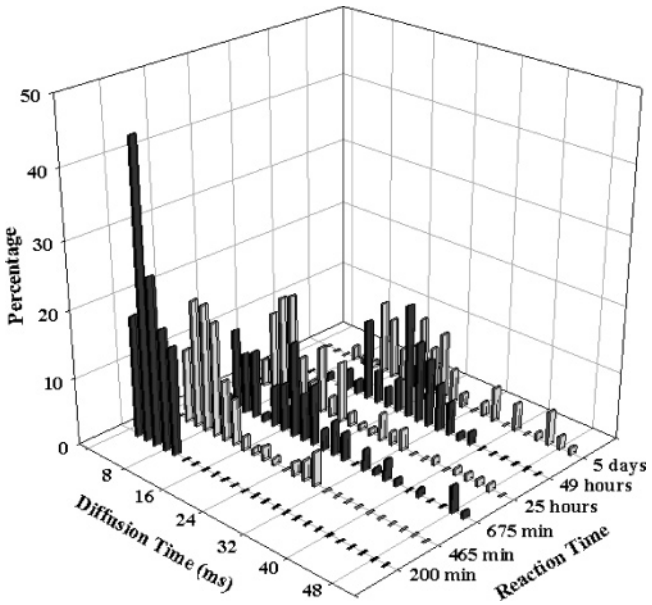

FIGURE 8: Distribution of diffusion times of polymerizing AT as a function of incubation time at 45 °C: 200 min, 465 min, 675 min, 25 h, 49 h, and 5 days.

the time dependence of polymerization, as measured by changes in diffusion time distribution, are consistent with the results of previous ensemble studies (*26*, *50*), the FCS studies provide the first detailed information regarding the size distribution of AT polymers.

AT polymerization at 45 °C proceeds in a heterogeneous manner, as shown by the time course of diffusion time distribution (Figure 8). Such distributions are generated by counting the number of diffusion time intervals obtained from the autocorrelation decay profiles (e.g., 0−2, 2−4, 4−6 ms, etc.). At an early stage of the reaction (e.g., 200 min), the distribution is dominated by a species whose diffusion time is about 4 ms, whereas at longer reaction times the distribution becomes broader and the center of the distribution shifts toward longer diffusion times. For example, at 465 min, the concentration of the monomer decreases to a level that is essentially undetectable by the current method, and there is a clear decrease in the number of the fast diffusing species, or short polymers, and a corresponding increase in the number of moderately slowly diffusing species, or longer polymers. At later reaction times, very slowly diffusing species (up to a diffusion time of ∼50 ms) are formed. Interestingly, however, these long chain polymers are only transiently stable and they disappear at a later time. After a 49-hour incubation, the polymers generated exhibit a relatively narrow distribution of diffusion times, centered at a diffusion time of ∼26 ms. According to previous studies (*29*), the reaction of AT polymerization under similar conditions should be virtually complete after about 42 h. However, the FCS results clearly show the reappearance of the species with very long diffusion times after incubating the sample continuously for 5 days. The mechanism leading to reappearance of these very long polymers is presently unclear.

It is of interest to directly relate diffusion times to polymer chain lengths. Several models are available for this purpose, which are applicable for different physical conditions of the polymers in solution (*51*−*55*). Depending on the properties of the systems of interest, the diffusion constant D of a polymer with N monomer units may exhibit rather complex dependence on N. According to the Rouse model (*51*), which was developed to describe the dynamics of dilute polymer solutions and is appropriate for the current studies, D is inversely proportional to N. Since the diffusion time, τ_D, is inversely proportional to D (*42*), N is proportional to τ_D. Applying this conclusion to, for example, the results obtained after 5 days of incubation of the 5 μM AT sample (Figure 8), and noting that AT monomer exhibits a characteristic diffusion time of ∼2 ms, the observed distribution of diffusion times between 16 and 28 ms corresponds to a chain length distribution of 8−14 monomer units.

DISCUSSION

FCS is a powerful technique for the study of heterogeneous processes (*31*, *35*−*37*), such as protein polymerization and aggregation, since it provides information unobtainable by ensemble methods. Here we apply FCS to investigate AT polymerization. Our results indicate that a lag phase precedes the formation of long polymers. The species formed toward the end of the lag phase at 45 °C exhibit a mean diffusion time of about 8−12 ms (Figure 7b), corresponding mainly to tetramers and hexamers, which appear to be required for formation of the longer polymers. Both the duration of the lag phase and the average length of the polymers formed are sensitive to temperature and concentration. For example, it takes about 500 min for long polymers (τ_D > 30 ms) to form at 45 °C, but at 55 °C they emerge in less than 80 min. Raising initial AT concentration has a similar effect. Moreover, higher temperature not only speeds up polymerization in general, but it also shifts the distribution of species toward considerably longer polymers. As expected, increasing AT concentration at a fixed temperature favors longer over shorter polymers.

Importantly, following the lag phase, long polymers form over a relatively short time interval (<15 min, Figure 7b), suggesting that the formation of long polymers encounters a relatively small activation barrier. Although this observation is in general agreement with a nucleation and growth model (*56*) whereby longer polymers form via the condensation of two shorter polymers, our results also show that the "nucleus" is not unique. Different nuclei can be formed, depending on the time, temperature, and perhaps other variables (e.g., pH). Such heterogeneity with respect to nucleation is one manifestation of the highly heterogeneous nature of AT polymerization, as indicated by the distributions of the diffusion times at discrete reaction times (Figure 8). The most populous species have 8 to 16 monomer units, consistent with a recent electron microscopic study, suggesting that stable AT polymers contain 7 to 14 monomers (*30*).

Interestingly, very long polymers (e.g. those with τ_D > 40 ms) are only transiently populated when AT is incubated at 45 °C. Moreover, polymerization appears not to reach equilibrium even after 49 h, with the appearance and disappearance of longer aggregates continuing for a prolonged period of time. The origins of this oscillating behavior are not clear. One possibility is that these very long polymer species further condense to form truly large aggregates that we do not detect, either because they precipitate or because they simply diffuse too slowly. Although this possibility cannot be ruled out entirely, we do not believe it is the main

mechanism leading to the disappearance of the very long polymers that we did observe, for two reasons. First, no visible precipitation was detected, even after incubating the sample (at 5 μM) for 5 days. Second, the amplitude of the autocorrelation function, $G(0)$, which is inversely proportional to the average number of fluorescent molecules, residing in the excitation confocal volume, increases by nearly a factor of 10 over 49 h (Figure 2), a period which coincides with the formation of a distribution of polymeric species with 8 to 16 monomer units (Figure 8). Thus, there is no obvious loss of sample mass over the course of the experiment. The more likely explanation of the oscillating behavior is that the observed long polymers are energetically not stable and break up to yield shorter polymers, via processes that are not simple reversals of formation steps and are perhaps initiated by random local conformational changes.

The results of the FCS studies presented here both elaborate and alter our understanding of AT polymerization, which has heretofore been based completely on studies at the ensemble level (*26*, *28*, *29*). In particular, our studies demonstrate (a) the heterogeneity of the reaction, which the ensemble studies failed to reveal; (b) the abruptness of long polymer formation, in striking contrast to the suggestion from ensemble measurements that the elongation of short polymers is a gradual process (*29*), akin to the formation of monomeric α-helices (*57*); and (c) that equilibrium in the polymerization process is not achieved even after very long times (up to 5 days) of incubation, whereas ensemble measurements had suggested that the polymerization of AT at 45 °C is essentially over by about 42 h (*29*).

CONCLUSIONS

In summary, AT polymerization was studied in detail by using the FCS technique, demonstrating aspects of the dynamics and heterogeneity of serpin polymerization that are unobtainable by ensemble methods. Our results clearly show that a temperature-dependent lag phase precedes the formation of long polymers, that such formation proceeds via combinations of two shorter chains, and that some long polymers are populated only transiently.

REFERENCES

1. Carrell, R. W., and Boswell, D. R. (1986) *Proteinase Inhibitors* (Eds. Barrett, A. J., and Salvasen, G.) pp 403−420, Elsevier, Amsterdam, The Netherlands.
2. Gettins, P., Patston, P. A., and Schapira, M. (1993) The role of conformational change in serpin structure and function, *BioEssays 15*, 461−467.
3. Carrell, R. W., and Stein, P. E. (1996) The biostructural pathology of the serpins: critical function of sheet opening mechanism, *Biol. Chem. Hoppe-Seyler 377*, 1−17.
4. Potempa, J., Korzus, E., and Travis, J. (1994) The serpin superfamily of proteinase inhibitors: structure, function, and regulation, *J. Biol. Chem. 269*, 15957−15960.
5. Lomas, D. A., and Mahadeva, R. (2002)α_1-Antitrypsin polymerization and the serpinopathies: pathobiology and prospects for therapy, *J. Clin. Invest. 110*, 1585−1590.
6. Baumann, U., Huber, R., Bode, W., Grosse, D., Lesjak, M., and Laurell, C. B. (1991) Crystal structure of cleaved human α_1-antichymotrypsin at 2.7 Å resolution and its comparison with other serpins, *J. Mol. Biol. 218*, 595−606.
7. Mourey, L., Samama, J. P., Delarue, M., Petitou, M., Choay, J., and Moras, D. (1993) Crystal structure of cleaved bovine antithrombin III at 3·2 Å resolution, *J. Mol. Biol. 232*, 223−241.
8. Wei, A., Rubin, H., Cooperman, B. S., and Christianson, D. W. (1994) Crystal structure of an uncleaved serpin reveals the conformation of an inhibitory reactive loop, *Nat. Struct. Biol. 1*, 251−258.
9. Elliot, P. R., Stein, P. E., Bilton, D., Carrell, R. W., and Lomas, D. A. (1996)Structural explanation for the deficiency of S α_1-antitrypsin, *Nature Struct. Biol. 3*, 676−681.
10. Loebermann, H., Tokuoka, R., Deisenhofer, J., and Huber, R. (1984) Human α_1-proteinase inhibitor: crystal structure analysis of two crystal modifications, molecular model and preliminary analysis of the implications for function, *J. Mol. Biol. 177*, 531−557.
11. Mottonen, J., Strand, A., Symersky, J., Sweet, R. M., Danley, D. E., Geoghegan, K. F., Gerard, R. D., and Goldsmith, E. J. (1992) Structural basis of latency in plasminogen activator inhibitor-1, *Nature 355*, 270−273.
12. Carrell, R. W., Stein, P. E., Wardell, M. R., and Fermi, G. (1994)-Biological implications of a 3 Å structure of dimeric antithrombin, *Structure 2*, 257−270.
13. Stein, P. E., and Carrell, R. W. (1995) What do dysfunctional serpins tell us about molecular mobility and disease? *Nat. Struct. Biol. 2*, 96−113.
14. Carrell, R. W., Lomas, D. A., Sidhar, S., and Foreman, R. (1996) Alpha1-antitrypsin deficiency: A conformational disease, *Chest 110*, 243S−247S.
15. Chang, W.-S. W., Whisstock, J., Hopkins, P. C. R., Lesk, A. M., Carrell, R. W., and Wardell, M. R. (1997) Importance of the release of strand 1C to the polymerization mechanism of inhibitory serpins, *Protein Sci. 6*, 89−98.
16. Bottomley, S. P., and Chang, W.-S. W. (1997) The effects of reactive centre loop length upon serpin polymerisation, *Biochem. Biophys. Res. Commun. 241*, 264−269.
17. Mast, A. E., Enghild, J. J., and Salvesen, G. (1992) Conformation of the reactive site loop of alpha1-proteinase inhibitor probed by limited proteolysis, *Biochemistry 31*, 2720−2728.
18. Lomas, D. A., Evans, D. L., Finch, J. T., and Carrell, R. W. (1992) The mechanism of Z α_1-antitrypsin accumulation in the liver, *Nature 357*, 605−607.
19. Mahadeva, R., Chang, W.-S. W., Dafforn, T. R., Oakley, D. J., Foreman, R. C., Calvin, J., Wright, D. G. D., and Lomas, D. A. (1999) Heteropolymerization of S, I, and Z α_1-antitrypsin and liver cirrhosis, *J. Clin. Invest. 103*, 999−1006.
20. Sivasothy, P., Dafforn, T. R., Gettins, P. G., and Lomas, D. A. (2000) Pathogenic α_1-antitrypsin polymers are formed by reactive loop-β-sheet A linkage, *J. Biol. Chem. 275*, 33663−33668.
21. Sveger, T. N. (1976) Liver disease in alpha1-antitrypsin deficiency detected by screening of 200,000 infants, *Engl. J. Med. 294*, 1316−1321.
22. Eriksson, S., Carlson. J., and Velez, R. N. (1986) Risk of cirrhosis and primary liver cancer in alpha1-antitrypsin deficiency, *Engl. J. Med. 314*, 736−739.
23. Carrell, R. W., Jeppsson, J.-O., Laurell, C.-B., Brennan, S. O., Owen, M. C., Vaughan, L., and Boswell, D. R. (1982) Structure and variation of human α_1-antitrypsin, *Nature (London) 298*, 329−334.
24. Eriksson, S. (1965) Studies in alpha1-antitrypsin deficiency, *Acta Med. Scand. Suppl. 432*, 1−85.
25. Lomas, D. A., Evans, D. L., Stone, S. R., Chang, W.-S. W., and Carrell, R. W. (1993) Effect of the Z mutation on the physical and inhibitory properties of alpha1-antitrypsin, *Biochemistry 32*, 500−508.
26. Crowther, D. C., Serpell, L. C., Dafforn, T. R., Gooptu, B., and Lomas, D. A. (2003) Nucleation of α_1-antichymotrypsin polymerization, *Biochemistry 42*, 2355−2363.
27. Lomas, D. A., Finch, J. T., Seyama, K., Nukiwa, T., and Carrell, R. W. (1993) Alpha1-antitrypsin Siiyama (Ser53→Phe). Further evidence for intracellular loop-sheet polymerization, *J. Biol. Chem. 268*, 15333−15335.
28. James, E. L., and Bottomley, S. P. (1998)The mechanism of α_1-antitrypsin polymerization probed by fluorescence spectroscopy, *Arch. Biochem. Biophys. 356*, 296−300.
29. Dafforn, T. R., Mahadeva, R., Elliott, P. R., Sivasothy, P., and Lomas, D. A. (1999) A kinetic mechanism for the polymerization of α_1-antitrypsin, *J. Biol. Chem. 274*, 9548−9555.
30. Devlin, G. L., Michelle, K. M. C., Howlett, G. J., and Bottomley, S. P. (2002) Acid denaturation of α_1-antitrypsin: characterization of a novel mechanism of serpin polymerization, *J. Mol. Biol. 324*, 859−870.

31. Tjernberg, L. O., Pramanik, A., Björling, S., Thyberg, P., Thyberg, J., Nordstedt, C., Berndt, K. D., Terenius, L., and Rigler, R. (1999) Amyloid β-peptide polymerization studied using fluorescence correlation spectroscopy, *Chem. Biol. 6*, 53−62.
32. Pitschke, M., Prior, R., Haupt, M., and Riesner, D. (1998) Detection of single amyloid beta-protein aggregates in the cerebrospinal fluid of Alzheimer's patients by fluorescence correlation spectroscopy, *Nature Med. 4*, 832−834.
33. Magde, D., Elson, E. L., and Webb, W. W. (1972) Thermodynamic fluctuations in a reacting system-measurement by fluorescence correlation spectroscopy, *Phys. Rev. Lett. 29*, 705−711.
34. Magde, D., Elson, E. L., and Webb, W. W. (1974) Fluorescence correlation spectroscopy. II. An experimental realization, *Biopolymers 13*, 29−61.
35. Vercammen, J., Maertens, G., Gerard, M., De Clercq, E., Debyser, Z., and Engelborghs, Y. (2002) DNA-induced polymerization of HIV-1 integrase analyzed with fluorescence fluctuation spectroscopy, *J. Biol. Chem. 277*, 38045−38052.
36. Bark, N., Földes-Papp, Z., and Rigler, R. (1999) The incipient stage in thrombin-induced fibrin polymerization detected by FCS at the single molecule level, *Biochem. Biophys. Res. Commun. 260*, 35−41.
37. Björling, S., Kinjo, M., Földes-Papp, Z., Hagman, E., Thyberg, P., and Rigler, R. (1998) Fluorescence correlation spectroscopy of enzymatic DNA polymerization, *Biochemistry 37*, 12971−12978.
38. Weston, K. D., and Buratto, S. K. (1998) Millisecond intensity fluctuations of single molecules at room temperature, *J. Phys. Chem. A 102*, 3635−3638.
39. Hess, S. T., Huang, S., Heikal, A. A., and Webb, W. W. (2002) Biological and chemical applications of fluorescence correlation spectroscopy: A review, *Biochemistry 41*, 697−705.
40. Nishimura, G., Rigler, R., and Kinjo, M. (1997) Number analysis of fluorescence correlation spectroscopy for the cleaving process of fluorescence labeled DNA, *Bioimaging 5*, 129−133.
41. Weidemann, T., Wachsmuth, M., Tewes, M., Rippe, K., and Langowski, J.(2002) Analysis of ligand binding by two-colour fluorescence cross-correlation spectroscopy, *Single Mol. 3*, 49−61.
42. Chattopadhyay, K., Saffarian, S., Elson, E. L., and Frieden, C. (2002) Measurement of microsecond dynamic motion in the intestinal fatty acid binding protein by using fluorescence correlation spectroscopy, *Proc. Natl. Acad. Sci. U.S.A. 99*, 14171−14176.
43. Corrie, J. E. T., and Craik, J. S. (1994) Synthesis and characterization of pure isomers of iodoacetamidotetramethylrhodamine, *J. Chem. Soc., Perkin Trans. 1*, 2967−2973.
44. Lagerkvist, A. C., Földes-Papp, Z., Persson, M. A. A., and Rigler, R. (2001) Fluorescence correlation spectroscopy as a method for assessment of interactions between phage displaying antibodies and soluble antigen, *Protein Sci. 10*, 1522−1528.
45. Aragón, S. R., and Pecora, R. (1976) Fluorescence correlation spectroscopy as a probe of molecular dynamics, *J. Chem. Phys. 64*, 1791−1803.
46. Eigen, M., and Rigler, R. (1994) Sorting single molecules: application to diagnostics and evolutionary biotechnology, *Proc. Natl. Acad. Sci. U.S.A. 91*, 5740−5747.
47. Luo, Y., Zhou, Y., and Cooperman, B. S. (1999) Antichymotrypsin interaction with chymotrypsin. Intermediates on the way to inhibited complex formation, *J. Biol. Chem. 274*, 17733−17741.
48. Devlin, G. L., Carver, J. A., and Bottomley, S. P. (2003) The selective inhibition of serpin aggregation by the molecular chaperone, α-Crystallin, indicates a nucleation-dependent specificity, *J. Biol. Chem. 278*, 48644−48650.
49. Wilkins, D. K., Grimshaw, S. B., Receveur, V., Dobson, C. M., Jones, J. A., and Smith, L. J. (1999) Hydrodynamic radii of native and denatured proteins measured by pulse field gradient NMR techniques, *Biochemistry 38*, 16424−16431.
50. Lomas, D. A., Elliott, P. R., Chang, W.-S. W., Wardell, M. R., and Carrell, R. W. (1995) Preparation and characterization of latent α_1-antitrypsin, *J. Biol. Chem. 270*, 5282−5288.
51. Rouse, P. E. (1953) A theory of the linear viscoelastic properties of dilute solutions of coiling polymers, *J. Chem. Phys. 21*, 1272−1280.
52. Zimm, B. H. (1956) Dynamics of polymer molecules in dilute solution: viscoelasticity flow birefringence and dielectric loss, *J. Chem. Phys. 24*, 269−278.
53. de Gennes, P. G. (1971) Reptation of a polymer chain in the presence of fixed obstacles, *J. Chem. Phys. 55*, 572−579.
54. Tothova, J., Lisy, V., and Zatovsky, A. V. (2003) Long-time tails in the dynamics of Rouse polymers, *J. Chem. Phys. 119*, 13135−13137.
55. Dua, A., and Cherayil, B. J. (2000) Chain dynamics in steady shear flow, *J. Chem. Phys. 112*, 8707−8714.
56. Zhao, D., and Moore, J. S. (2003) Nucleation-elongation: a mechanism for cooperative supramolecular polymerization, *Org. Biomol. Chem. 1*, 3471−3491.
57. Huang, C.-Y., Getahun, Z., Zhu, Y., Klemke, J. W., DeGrado, W. F., and Gai, F. (2002) Helix formation via conformation diffusion search, *Proc. Natl. Acad. Sci. U.S.A. 99*, 2788−2793.

BI048662E